First-principles study of rare earth adsorption at β-Si_3N_4 interfaces

Gayle S. Painter,[1,*] Frank W. Averill,[1,2] Paul F. Becher,[1] Naoya Shibata,[3] Klaus van Benthem,[4,†] and Stephen J. Pennycook[1]
[1]*Materials Science and Technology Division, Oak Ridge National Laboratory, Oak Ridge, Tennessee 37831, USA*
[2]*Department of Materials Science and Engineering, University of Tennessee, Knoxville, Tennessee 37996-0750, USA*
[3]*Institute of Engineering Innovation, University of Tokyo, Yayoi, Tokyo 113-8656, Japan*
[4]*Center for Nanophase Materials Sciences, Oak Ridge National Laboratory, Oak Ridge, Tennessee 37831, USA*
(Received 25 August 2008; revised manuscript received 5 November 2008; published 17 December 2008)

Structural characterization of rare earth adsorption at surfaces or interfaces of β-Si_3N_4 grains within silicon nitride ceramics has recently been reported by three different groups using *Z*-contrast scanning transmission electron microscopy (STEM) imaging. Here we report the electronic structure basis for these observations and discuss the origin of similarities and differences among the lanthanides characterized in that work. Along with the features that are well described by a first-principles cluster and surface slab models, we identify those differences in the experiment and theory that warrant further investigation. Stereochemical bonding factors are found to determine adsorption site preferences as opposed to ionic size effects. The set of possible bond sites is a characteristic of the β-Si_3N_4 interface; however the strength of the rare earth–interface bonding is determined by the electronic structure of the nitride surface and the specific adsorbate. This is the principal factor controlling the effects of dopants on the $\alpha \rightarrow \beta$ phase transformation and on the β-Si_3N_4 grain growth at high temperature as well as the subsequent microstructure of the ceramic.

DOI: 10.1103/PhysRevB.78.214206 PACS number(s): 71.55.Jv, 81.05.Je, 68.55.Ln, 73.90.+f

I. INTRODUCTION

Additions of metallic compounds are widely used in ceramic processing to promote densification of the powder compacts during sintering.[1–5] Atoms of the sintering additions often reside largely within regions separating the crystalline grains. These regions can take the form of disordered amorphous nanometer scale intergranular films (IGFs) and larger amorphous multigrain pockets that result from the reaction between additives and other constituents during densification at elevated temperatures. Some of these species can segregate to grain surfaces and adsorb there according to the chemical driving force and interaction with other atoms in the glass. After densification, these grain-boundary phases are known to greatly influence the resulting microstructure and mechanical properties of ceramics,[6–9] and it is thus important to understand the mechanism and effects of dopant adsorption at internal interfaces.

Silicon nitride (Si_3N_4) ceramics have become a model material for basic and applied studies of ceramics[10–13] due to the considerable degree to which they have been characterized, as well as their importance as structural and electronic materials. Rare earth (RE) oxide additions are observed to strongly affect the $\alpha \rightarrow \beta$ phase transformation, which occurs during densification[14,15] and the anisotropic shape of β-Si_3N_4 grains that grow in the high-temperature sintering stage,[16–22] suggesting that they affect the attachment of nitride growth fragments during Si_3N_4 crystalline growth and do so with specific surface sensitivity. Since the morphology of the growing grains depends upon RE type and grain aspect ratios are important to fracture toughness of the ceramic,[17] dopant selection provides a way to control the ceramic's macroscopic physical properties. It is thus important to obtain a basic understanding of RE adsorption on β-Si_3N_4 prism planes and the reasons for observed differences among the RE series.

Until recently[5] little was known about the distribution of rare earths within IGFs mainly due to the difficulties posed for chemical probes by both the very small thickness (e.g., 1–2 nm) of the IGF and the need to image the RE atoms. Recently RE adsorption at the glass/silicon nitride grain interface has been determined through high-angle annular dark-field (also known as *Z*-contrast) scanning transmission electron microscopy (STEM) imaging carried out by three research groups[23–28] generally using samples from the same source.[29] Here, we report first-principles calculations that describe details of the adsorption behavior of La, Lu, and Gd at the prism plane surface of β-Si_3N_4 [shown in Fig. 1(a)]. The actual computational models used in this work are pictured in Figs. 1(b) and 1(c). Electronic structure factors that underlie the observed differences in RE segregation and adsorption behavior are described. Stable interfacial bond sites for specific rare earths are determined by minimizing the total energy of the system through atom relaxations according to calculated forces. The relative binding energies of the REs at different surface sites identify site preferences, and comparisons of the bond strengths of different rare earths in similar sites give insight into relative adsorption or desorption strengths that relate directly to effects on the phase transformation and grain growth. Finally, analysis of the calculated electronic structure characterizes the nature of the adsorbate/substrate bond, which has been shown earlier to explain differences in the effects of RE additions on phase transitions[14] and on grain growth anisotropy.[30]

II. METHODS

Various theoretical methods have been used[31–35] to model and understand intergranular behavior, motivated by the fact that these nanoscale films effectively control macroscopic ceramic behavior. For problems that require an understanding in terms of the electronic structure and bonding, density-

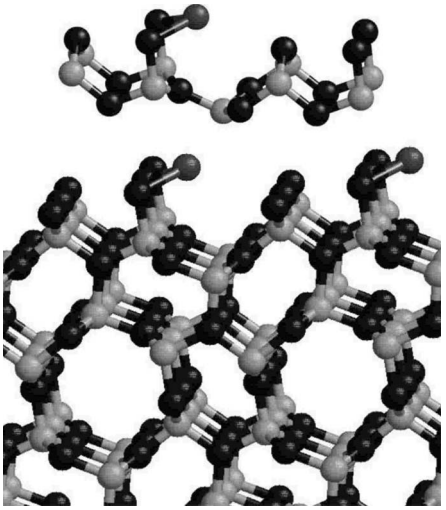

(a)

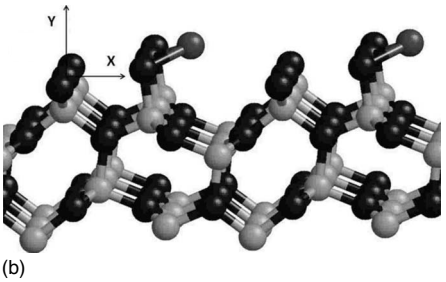

(b)

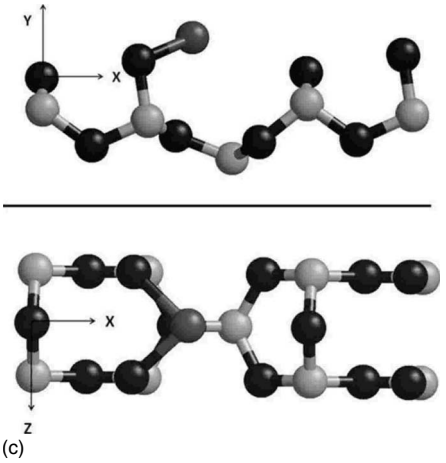

(c)

FIG. 1. (a) The β-Si_3N_4 crystal structure viewed slightly off normal to the basal plane and across the edge of the $[11\bar{2}0]$ prism plane terminating with N atoms and one adsorbed RE atom in each surface unit cell. The actual computational models used in this work are pictured in parts (b) and (c). The inset of (a) is an atomic cluster model of this interface shown with a RE adsorbate. (b) The β-Si_3N_4 model surface with an adsorbed RE within each surface unit cell along the prism plane. Also shown are the atoms underneath the surface which are included in the VASP surface slab calculations as well as the local coordinate system for that model. The horizontal slice shown here is infinitely replicated in the z direction. (c) Side and top views of the 23 atom cluster model of the surface with its local coordinate system. The 1.06 nm length of the cluster gives the scale of the system. The x direction is the $[10\bar{1}0]$ of the β-Si_3N_4 lattice, the y direction represents the $[11\bar{2}0]$ and the z direction the [0001].

TABLE I. The computed (theor.) lattice constants and cohesive energies (BE) of LaN, GdN, and LuN compared with experiment (expt.). The VASP PAW pseudopotentials of Gd and Lu include the atomic $5s$ and $4f$ levels in the core. The experimental values for LaN and GdN are as reported in Refs. 40 and 41, respectively. The experimental lattice constant of LuN is given in Ref. 42. The present authors were unable to find an experimental value for the cohesive energy of LuN.

	LaN	GdN	LuN
a (Å) (theor.)	5.31	4.98	4.76
a (Å) (expt.)	5.31	4.99	4.76
BE (eV) (theor.)	−12.45	−12.53	−12.99
BE (eV) (expt.)	−10.93	−12.40	*xx*

functional methods are especially advantageous, particularly considering the complexity of such systems. The formal basis of this work is the semilocal generalized gradient exchange-correlation approximation of Perdew, Burke, and Ernzerhof (GGA-PBE).[36] Most properties of glassy intergranular films are dominated by very localized bonding without long-range order, and in this case it is advantageous to focus on a localized structural model (cluster) comprised of the atoms that are of central importance and a limited number of neighboring atoms. The principal requirement for the cluster model to adequately describe the system is that the influence of atoms outside the cluster effectively subtract out in calculating quantities of interest. Nevertheless, in order to assess the adequacy of our finite atom cluster model [Fig. 1(c)], additional calculations were performed using an infinite slab of finite thickness composed of the first approximately six layers of atoms [Fig. 1(b)] from the prism plane of β-Si_3N_4.

In this work, we solve the spin-polarized GGA-PBE equations using one of two different methods depending upon the theoretical model being employed and the purpose of the calculation. The surface slab calculations were carried out using the Vienna *ab initio* Simulation Package (VASP) (Ref. 37) and the projector augmented-wave (PAW) method.[38] Atoms in adjacent slabs along the y direction [see Fig. 1(b)] were separated by at least 8 Å so any spurious interaction between slabs was minimized. Similarly, the absorbed rare earth atoms on the simulated surface occupy only every other symmetry related site in the z direction and are therefore separated by about 5.8 Å. Brillouin-zone integration was accomplished by the Monkhorst-Pack method[39] using an $11 \times 1 \times 11$ point grid. The plane-wave cutoff was set at 400 eV, where convergence was achieved.

The VASP PAW pseudopotentials included the following atomic orbitals in their respective valences: $Si(3s^2,3p^2)$, $N(2s^22p^3)$, $La(5s^2,5p^6,6s^2,5d^1)$, $Gd(5p^6,6s^2,5d^1)$, and $Lu(5p^6,6s^2,5d^1)$. As a check of the RE potentials, the lattice constants and cohesive energies of the RE-nitride solids were computed using the VASP PAW method and are compared with experiment[40–42] in Table I. It can be seen that the computed lattice constants are within 1% of the experimental values and the largest error in the cohesive energy is about 14%. As a further check of the RE pseudopotentials,

a few calculations reported here employed pseudopotentials with larger valences that include the $5s$ and $4f$ levels of Gd and Lu: Gd$(5s^2,5p^6,4f^7,6s^2,5d^1)$ and Lu$(5s^2,5p^6,4f^{14},6s^2,5d^1)$.

For each of the finite atom cluster models, the GGA-PBE equations were solved using the self-consistent partial-wave (SCPW) method.[43,44] This technique is a linear variational approach that is particularly well suited for systems with low symmetry and covalent bonding. Basis functions for each atom include atomic orbitals with radial parts that are in numerical form and a set of additional "tail" orbitals (Gaussian functions) of each angular momentum number. The atomic cores are explicitly treated. As a further cross-check of methods and models, the finite atom cluster models were also evaluated using the VASP and PAW methods with the finite cluster inserted into an infinite array of repeating rectangular "supercells" where Brillouin-zone integration is limited to a single point ($k=0$). The cells were constructed large enough so that atoms in adjacent clusters were never closer to each other than 9 Å. As was done in the VASP surface calculation, the plane-wave cutoff was set at 400 eV.

This study focuses on the interaction of rare earth atoms with the $[11\bar{2}0]$ prism planes of β-Si_3N_4 because it is this interface that is most important in the response of β-Si_3N_4 to the effects of RE adsorption. The $[11\bar{2}0]$ grain surfaces are prevalent and are quite smooth even at the atomic level, with few steps/facets for atoms to attach to. On the other hand, the [0001] "cap" is highly facetted, which promotes attachment of atoms. In Fig. 1(a), this surface of β-Si_3N_4 is viewed in perspective for an N-terminated prism plane, with alternating parallel channels that are defined by rows of terminal N and Si atoms. A surface unit cell based cluster is shown in the inset. As the results will show, electronic structure effects from distant atoms can be omitted as far as the qualitative structural properties are concerned. Truly quantitative calculations of RE positions and binding energies will require the inclusion of the interaction of the RE atoms with the IGF, as well as the β-Si_3N_4 grain surface. As will be shown below, the experimentally determined positions of the REs on the grain surface suggest that for those RE sites producing the most intense STEM images, the interaction of the RE with the grain surface appears to be more important than the interaction of the RE with the IGF.

This surface was initially selected for first-principles studies because it is characterized by a high density of undercoordinated N atoms considered likely sites for RE binding (as in fact they are for Si attachment in the grain growth process.) This *a priori* choice proved to be the configuration observed during the first STEM experiments of the La-doped Si_3N_4 ceramic.[23] The structural models in this work are based on unit cells for this prism surface of β-Si_3N_4 and are shown with their local coordinate systems in Figs. 1(b) and 1(c).

Stable bonding positions of a given RE were determined by calculating the restoring force field experienced by the adsorbate and allowing its relaxation into locally stable sites. Relative strengths of binding among the series were calculated by differencing the total energies of the host with and without the RE atom; i.e., RE binding energy$=E$(host+RE) $-E$(host)$-E$(RE). The RE atom energies are computed for spherically symmetrized atoms. Nevertheless, the most accurate results are structural, such as the adsorbate positions on the surface, and it is these that we compare to experiment.

III. FIRST-PRINCIPLES RESULTS AND COMPARISON WITH EXPERIMENT

In the present calculations, the host cluster for the RE was kept fixed with the experimentally determined[45] structural parameters of β-Si_3N_4. Here the x and y coordinates of the RE were relaxed in the $z=0$ plane that bisects the unit cell [see Fig. 1(c)] and contains the RE. Local total-energy minima (stable bond sites) and maxima (unstable equilibriums) were identified by vanishingly small restoring forces (<0.05 eV/Å) on the RE.[44]

Calculations showed that relaxation of N atoms in the x and y directions causes rotations of RE-N bonds and, consequently, a shift of the RE atoms from nucleation site B, which is in disagreement with the experimental observations. This effect is particularly pronounced for the small cluster models [Fig. 1(c)] where the N atoms were found to rotate as much as 25° from the solid-state lattice positions due largely to the unphysical "openness" of the B site in these simple cluster models. In the atom cluster models, this can be remedied by adding additional atoms from the surface to the cluster so the unnatural openness of the B site is appropriately filled. However, a 15° rotation is observed even in the surface slab model [Fig. 1(b)]. One suspects that the mobility of the RE and surface N atoms is further restricted by their interaction with the IGF although theoretical proof of this will require the rather daunting addition of the disordered nature of the atomic structure of the IGF in future studies. Therefore, for consistency within the present cluster and surface slab models, we chose to leave all host atoms frozen at their infinite lattice positions.

Calculated equilibrium adsorption sites in the cluster and surface slab models are illustrated in Fig. 2(a). In Fig. 2(b), the free energy of the slab surface model is displayed as a function of the x coordinate of the La atom as it moves down the x axis within the surface unit cell. For each value of the x coordinate of La, its y coordinate was allowed to relax until the restoring force in that direction was essentially zero (<0.05 eV/Å). Although the results given in Fig. 2(b) were obtained for the surface slab model [Fig. 1(b)] of La absorption on the grain surface, a qualitatively similar curve was also found for the 23-atom cluster model [Fig. 1(c)] of the same system as well as for the Gd and Lu absorption models.

As can be seen in Table II, the positions of sites A, B, and M calculated for each RE are about the same regardless of which model (surface slab or atom cluster) is employed. The relative order of the RE binding energies of the sites ($E_A<E_B<E_M$; see Table III) is also the same although the actual values of these energies do differ particularly between the surface slab and atom cluster models. Two stable binding sites per cell were found in the $z=0$ plane common to every rare earth: one each in the large and small channels. Total-energy calculations (Table III) predict that the position in the small channel, designated as A in Fig. 2, is more stable than

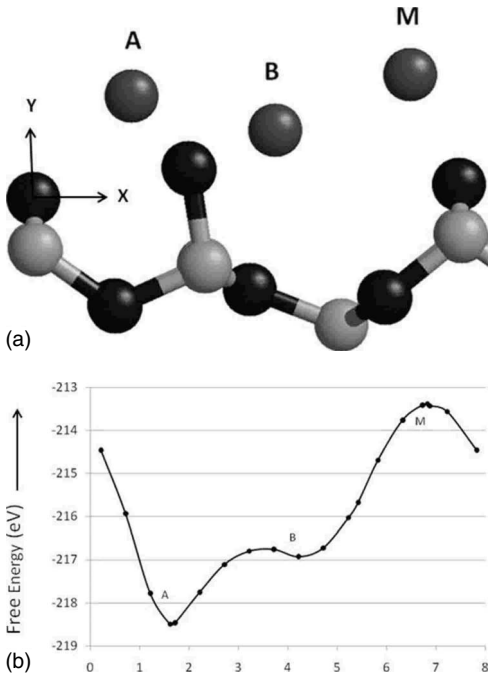

FIG. 2. (a) Surface decoration pattern of RE atom adsorbed on the nitride prism plane (all in $z=0$ plane). The coordinate system is defined in Fig. 1. RE absorption sites A and B are stable RE equilibrium sites in the atom cluster and surface slab models. Site M is an unstable equilibrium in these models and has only been observed experimentally in the case of La and not in Gd or Lu. It is hypothesized in the text that for La, site M may be stabilized by the interaction of that RE with the IGF. (b) Free energy (eV) of the surface unit cell in the surface slab model as a function of the x coordinate (Å) of the La atom as La moves in the $z=0$ plane above the grain surface. The relative stabilities of sites A, B, and M in this model can be clearly seen.

site B found in the large channel. A third site in the large channel (labeled M and theoretically unstable in these models) is also observed experimentally for La. This perhaps reflects not only reduced ability for the lone double-bonded surface N atom to bond with Gd and Lu in that site but also the lower concentrations of Gd and Lu (compared with La) as predicted by the differential binding-energy (DBE) model.[30]That model predicts an increasing potential for segregation to a nitride interface in the order Lu$<$Gd$<$La. Since the relevant N atom near the M site has only a single unoccupied bond as a surface species, it is expected to thereby show lower bond-formation ability than the pair of single-bonded N atoms in the adjacent anion row. The order in energetic stability of these sites, viz., $E_A<E_B<E_M$, holds for each RE. The Lu, Gd, and La set studied here span the range of atomic radii in the lanthanides, and thus this ordering illustrates the secondary role of size effects, compared to stereochemistry, in the RE-surface bonding. Experimental adsorption patterns obtained for the La-doped, Gd-doped, and Lu-doped samples[27] show that the adsorption along the prism plane, while periodic, differs for the various RE and also deviates from expectations based on size alone. Direct experimental STEM images for Gd-doped and Lu-doped silicon nitride samples are shown in Figs. 3(a) and 3(b), respectively, where ground-state cluster models are superimposed and repeated along the x axis. While the calculated bonding sites agree very well with the images for Gd (as they did for La), there are differences for Lu. The A sites correspond very well to the brighter spots in the image; however, the B sites that are occupied (some appear vacant) frequently appear closer to the A sites than predicted. Recall that the higher atomic number for Lu yields a more intense image than Gd. Yet some cells appear to show a low population of B sites, and this is expected for the diminished segregation of Lu from the triple pockets into the IGF and hence to the interface according to the DBE theory.

From these results it is clear that size effects are secondary to the chemical bonding factors, in which they are implicit. First, size considerations would place the adsorbate near the center of sites of larger open volume, which for the prism plane correspond to the larger B channel shown in Fig. 2. However, both the STEM imaging and the calculations show that the RE attachment site B is displaced away from the center of this large channel and falls closer to the side adjacent to the single-bonded surface N pair (see also Fig. 3). Second, the more stable bond site (A) is over the *small* channel near this same N pair, contrary to expectations based on size considerations alone. This is most striking in the case of Lu, shown in Fig. 3(b), for which both experiment and theory show that occupancy of small channel A sites far outweighs that of the B sites. The intensity of B sites becomes quite low along some channels, whereas the A sites are consistently bright. The electronic structure explanation of the RE adsorption behavior has a straightforward basis in chemical bonding. For each type of rare earth, the preference for threefold bonding is satisfied by a set of three nitrogen atoms that make up near-anion neighbors at sites A and B (see Fig. 4).

The presence of the single-bonded pair of surface anions (N or possibly O) that divides the prism surface into small and large channels along the $[10\bar{1}0]$ (see Fig. 2) largely determines the observed decoration pattern of rare earths on the prism plane. In a traditional covalent-bonding picture, these single-bonded N atoms are chemically active, with two unfilled $2p$ orbitals each (in an atomic analysis).[46] The RE adsorbate (with three valence electrons) can then strongly coordinate with this pair of N surface atoms. Bridge bonding of the RE with this pair forms two surface bonds, while leaving a single unfilled orbital on each N. Thus occupancy of the same type of site in the adjacent unit cell (along the [0001] direction) by another RE will contribute to saturation of all the bonds (three) of each shared N. (A somewhat higher-energy configuration has both A and B sites occupied within the same unit cell.)

Why is the A site characterized by stronger RE bonding than the B site? Again the stereochemistry of the unsaturated surface N sites determines this behavior. The A and B sites are distinguished by the presence of a double-bonded N atom [in the next N row dividing the small and large (001) channels] that completes the threefold N group of the A-site. However the B site offers no additional unsaturated N atom that is near enough for strong binding with the RE. The nearest unsaturated N atom is about 3.4 Å away from the rare earth B site and thus interacts more weakly with it. A RE

TABLE II. Adsorbate positions (in Å) for La, Gd, and Lu on the prism plane of β-Si_3N_4. Coordinates (x,y) in the $z=0$ plane are measured from the surface N reference site (0,0) in Fig. 2. Positions (x,y) are given for the stable bond site (A) in the small channel, stable bond site (B) in the large channel, and the unstable equilibrium site (M) also in the large channel. Experimental measurements from groups at Oxford (Refs. 25 and 26) and Oak Ridge/University of Tokyo (OR/UT) (not previously published) are compared with calculated ground-state positions (theor) reported in this paper. The columns labeled VASP surface and VASP cluster are VASP PAW calculations for the surface and cluster models described in Figs. 1(b) and 1(c). The last column gives results for the SCPW method applied to the cluster model. The theoretical positions given in parentheses were computed using VASP PAW pseudopotentials which include the $5s$ and $4f$ electrons in the valence orbitals. The experimental numbers in square brackets are error bounds for the associated experimental positions. The relative energetic stability for each RE in these sites follows the trend $E_A<E_B<E_M$, where $E_i<0$. The experimental entries denoted by x are not observed or not reported.

	x coordinate (Å)				
RE/site	Expt. (Oxford)	Expt. (OR/UT)	Theor. (VASP surface)	Theor. (VASP cluster)	Theor. (SCPW cluster)
			La		
A	1.6	1.37[±0.31]	1.61	1.86	1.86
B	5.3	4.27[±0.42]	4.25	4.30	4.46
M	X	6.38[±0.30]	6.79	6.91	6.81
			Gd		
A	X	1.4	1.63(1.65)	1.77(1.82)	1.93
B	X	4.9	4.30	4.33(4.31)	4.26
M	X	X	6.82	6.97	6.72
			Lu		
A	1.9	1.61[±0.17]	1.64	1.77(1.77)	1.90
B	3.6	3.52[±0.23]	4.22	4.25(4.27)	4.29
M	X	X	6.64	7.03	6.96
	y coordinate (Å)				
RE/site	Expt. (Oxford)	Expt. (OR/UT)	Theor. (VASP surface)	Theor. (VASP cluster)	Theor. (SCPW cluster)
			La		
A	2.4	1.91[±0.25]	1.63	1.70	1.79
B	1.3	1.58[±0.26]	1.14	1.09	1.09
M	X	2.29[±0.26]	1.83	1.85	1.91
			Gd		
A	X	1.7	1.49(1.49)	1.54(1.55)	1.63
B	X	0.7	0.94	0.87(0.91)	1.07
M	X	X	1.83	1.85	1.89
			Lu		
A	1.8	1.50[±0.15]	1.36	1.39(1.41)	1.51
B	1.7	1.49[±0.13]	0.85	0.77(0.78)	0.82
M	X	X	1.72	1.84	1.80

at the B site can also form a third weaker bond to a near N atom in the plane below, however, it is already saturated (threefold bonded), as illustrated in Fig. 4.

The nature of the bonds that a RE forms with N atoms is emphasized in the quantum description of the La interface illustrated in Fig. 5, where *deformation densities* (the change in charge density due to La-interface cluster bonding) are shown. The deformation density is defined as

$$\rho_{\mathrm{dfm}}(\mathbf{r}) = \rho(\mathbf{r};\mathrm{Si_3N_4 + La}) - \rho(\mathbf{r};\mathrm{Si_3N_4}) - \rho(\mathbf{r};\mathrm{La}), \quad (1)$$

where the first term on the right is the total charge-density distribution of the La-doped interface cluster, the second term is the density of the undoped interface cluster, and the last term is the atomic density of the La. These charge densities are each obtained by summing over the squares of all occupied atom cluster model SCPW one-electron states

TABLE III. Theoretical binding energies (in eV) for La, Gd, and Lu on the prism plane of β-Si3N4 at three potential adsorption sites defined in Fig. 2 and specified in Table II. The RE binding energies were calculated by differencing the total energies of the host with and without the RE atom. The columns labeled VASP surface and VASP cluster are VASP PAW calculations for the surface and cluster models described in Fig. 1. The last column (SCPW cluster) gives results for the SCPW method applied to the cluster model. The binding energies given in parenthesis were computed using VASP PAW pseudopotentials which include the 5*s* and 4*f* electrons in the valence orbitals.

	RE binding energy (eV)		
RE/site	VASP surface	VASP cluster	SCPW cluster
	La		
A	−13.29	−11.61	−10.97
B	−11.88	−11.27	−10.42
M	−8.72	−7.68	−7.02
	Gd		
A	−12.42(−11.93)	−11.68(−10.15)	−9.68
B	−10.57	−11.19(−9.60)	−9.07
M	−7.09	−7.16	−6.22
	Lu		
A	−12.32	−10.37(−10.18)	−11.49
B	−10.20	−9.75(−9.57)	−10.67
M	−6.71	−5.55(−5.42)	−6.40

(weighted by the occupancy of each state), for example,

$$\rho_C(\mathbf{r}) = \Sigma_i n_i |\varphi_i(\mathbf{r})|^2, \tag{2}$$

where n_i is the occupation number of ith state φ_i of cluster C.

The deformation density then represents the change in charge density arising from the interface/La-atom interaction. Since it is a redistribution of conserved charge, the deformation density integrates to zero. From the charge redistributions shown in Fig. 5, it is clear that an ionic description is not completely accurate; i.e., there is a charge transfer from the bond region of La to the neighboring N but the N in turn use that charge to form *sp*-directed bonds toward the La atom. The two nitrogen atoms that are each single bonded to a Si atom (N2 and N3 in Fig. 5) form the dominant bond to La. The third N (N1 in Fig. 5) is bridge bonded to adjacent Si atoms and has one dangling bond that completes the trigonal N array that defines the *A* site. Rare earth occupancy of the *B* site also shows strong bonding with the same pair of singly coordinated N atoms. However, the only additional N atom that is near enough to participate in bonding at the *B* site is already threefold coordinated to Si sites and can participate only weakly in the RE-interface bond.

The calculated RE adsorption coordinates are compared with results from high-resolution aberration corrected STEM imaging[23,25,27,28] in Table II. The Oxford measurements involved averaging several (~30) images over a number of surface unit cells,[25] while the Oak Ridge National Laboratory/University of Tokyo (OR/UT) results are obtained by averaging positions each of which is extracted from one image. The position coordinates of both experi-

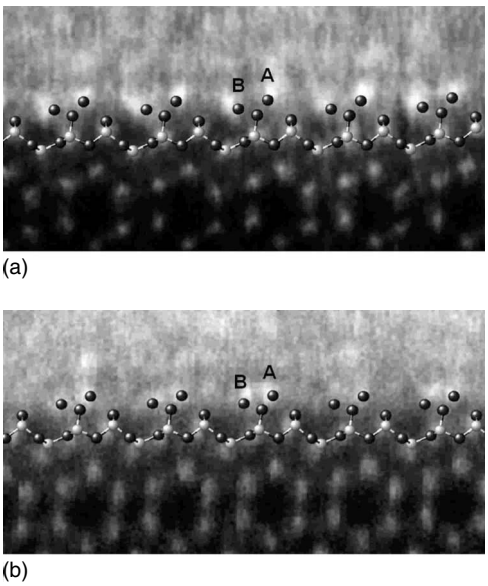

FIG. 3. Comparison of aberration corrected STEM images of RE adsorption at the prism planes of β-Si_3N_4 grains in silicon nitride ceramics and theory. In (a) Gd is the RE additive (as an oxide) and in (b) the RE is Lu. The array of hexagonal spots in the lower half of each panel originates from Si atom columns along the crystal *c* axis. The top row of Si (and terminal N) atoms is superimposed by translated atomic cluster models showing calculated RE adsorbates. The two bright spots that repeat with the period of the surface in the images correspond to RE in the pair of calculated stable *A* and *B* sites in the surface unit cell. These define the interface with the amorphous intergranular film that extends out and terminates on an adjacent grain interface with random orientation.

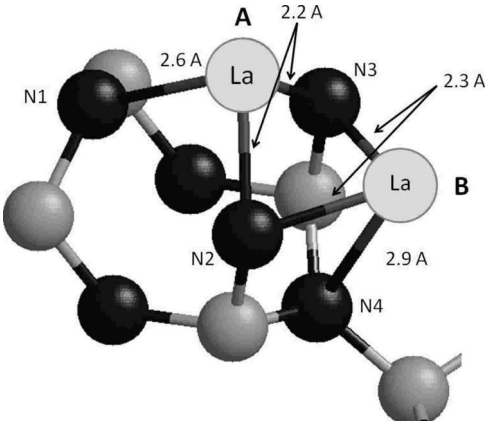

FIG. 4. Perspective view of primary adsorption sites *A* and *B* for RE=La defined by single-bonded anion pair on the $(11\bar{2}0)$ prism plane of β-Si_3N_4. Site *A* binding energy is stronger than that at *B* due to coordination factor: threefold RE-N bond set (2.2, 2.2, 2.6) of *A* versus that of (2.3, 2.3, 2.9) of *B*, all in Å. The added bond strength of site *A* appears to come from the N at 2.6 Å (i.e., N1) which has an unsaturated third bond to give to the RE, whereas the comparable N at 2.9 Å (i.e., N4) from *B* is fully saturated.

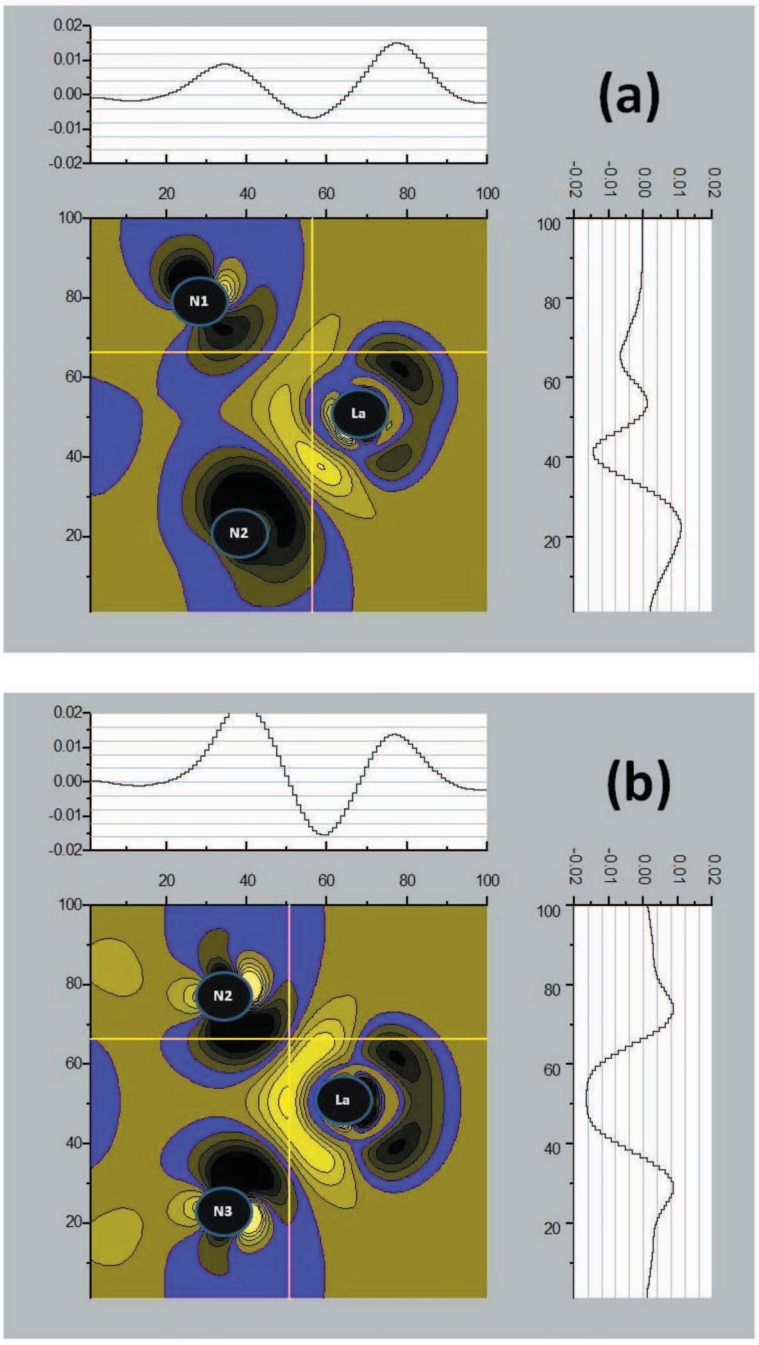

FIG. 5. (Color) Atom cluster model SCPW charge deformation densities for La adsorbed at the *A* interfacial site. In (a) the plane of the contours passes through the La atom (see Fig. 4) and the N atoms N1 and N2 are located at 2.6 and 2.2 Å, respectively, from the La. In (b) the plane passes through the La atom and both N at 2.2 Å (N2 and N3). The violet contour is the zero level contour and successive contours differ by ±0.004 units. The cutoffs for contours occur at −0.02 and +0.016. The line curves at the top and right sides are values along the intersecting cuts shown in the figures. The La atom bonds to the interface by transferring charge from its bond region to the nearby N atoms which in turn form directed *sp* bonds toward La. The especially large strength of the La bond to N2 and N3 is evidenced by the large charge transfer from La and the large directed *sp* bonds on N2 and N3.

mental groups have been transformed to our coordinate system (Fig. 1).

The theoretical results are the calculated equilibrium positions of each rare earth and for both the surface slab and atomic cluster models (Fig. 1). The VASP and SCPW cluster model positions are in very good agreement once account is taken of the vast differences in these two methodologies. The largest discrepancy is only about 0.2 Å. The VASP surface slab and VASP cluster model results in Table II are also in fair agreement although there are systematic differences showing that the additional atoms provided by the surface slab model do impact the exact locations of where the RE's sit on the surface. Even so, the simple atomic cluster model does appear to exhibit the important features giving, for example, the correct order for the energies of the three sites ($E_A < E_B < E_M$, Table III), and roughly the right coordinates for those positions (Table II). Nevertheless, the differences in energies of sites *A* and *B* (Table III) are consistently larger for the surface slab model indicating the secondary but quantitatively important effect of the underlying atoms included in the surface slab model but not the atom cluster model.

The La and Lu positions given by the two experimental groups are in fair agreement with each other considering the differences in STEM sensitivities and image processing. The largest difference between experimental results in Table II pertains to the *x* coordinate of the La *B* site (1.0 Å). The OR/UT images also show distinct occupancy of the *M* site for La but an absence for Gd and Lu. That this site is com-

puted to be unstable for both the slab and cluster models suggests that the La atom must obtain its stability at this location from its interaction with atoms in the IGF. The *M* site is not observed in the Oxford images perhaps because of its weak binding energy at that site. In a third study,[24] La was detected within the IGF; however no periodic ordering was observed at the grain boundaries. This may reflect the differing abilities of different STEM instruments to detect the interface adsorption of the lower mass La. The Gd experimental (OR/UT) and theoretical results are in reasonably good agreement for all sites, with a largest difference of 0.6 Å for the *x* coordinate of site *B*.

For the case of Lu additions, Oxford results show a distinct occupancy of the *B* site, as predicted by first principles; however Lu at that site is weakly imaged in the OR/UT results. As discussed earlier, segregation is predicted to be weak for Lu,[14,30] leading to a sparser population of these less stable *B* sites. The averaging procedure of the Oxford data is expected to enhance the images of the *B*-occupied sites, so the results are not so different in this regard. The Lu pair is clearly observed in the third study[24] and is assigned a separation of 1.43 ± 0.07 Å. This close proximity of the (A,B) pair compares with the larger Oxford and OR/UT value of ~1.7 Å; the separation of the *A* and *B* sites in *y* is only ~0.1 Å or less for both sets of data.

Table II and Fig. 3(b) show that the theoretical models for Lu additions are quite accurate for the more stable *A* site; however there are significant differences (as large as 0.7 Å) for the *B* site. While the position of the *A* site is quite close to that calculated from first principles, the *B* site appears much closer to the terminal N atoms than theory indicates. Since the theoretical structural models describe La and Gd very well, this variance for Lu suggests that some additional influence outside these models is present—specifically for Lu. The most obvious effect omitted in the modeling is that of the atoms in the glassy film, but why they would influence Lu more strongly than the other REs is not resolved at present. Replacement of the terminal N atoms by O atoms leads to rather small changes in the RE positions and does not explain the different position of the observed *B* site for Lu. Since the terminal (single-bonded) N atoms defining the small and large channels might be displaced, particularly during the STEM measurements, calculations were carried out for several displacements of the N positions. The corresponding adsorption position of the RE in the *B* site was then found to be displaced a little more to the center of the large channel. While such sites no doubt contribute to the measured images, further study is required to resolve the differences in this comparison. Overall the agreement between theory and experiment is rather good, suggesting that, with the possible exception of the Lu *B* sites, neighboring atoms in the glass play a secondary but not negligible role in determining the rare earth equilibrium positions.

In closing, it should be noted that VASP PAW results in Tables II and III show that inclusion of the 5*s* and 4*f* levels in the valence of the Gd and Lu pseudopotentials has only marginal effects upon the theoretical equilibrium positions of those atoms (Table II) but does produce a significant decrease in the Gd binding energies (Table III). The authors would have liked to have carried out additional calculations with these larger valence pseudopotentials, but they were not always able to obtain convergence in the resulting energy bands in the VASP code. This is of course only a technical computational issue that will no doubt be resolved in later versions of the VASP computer code. Since the focus of this work was on the equilibrium positions and not binding energies, the smaller valence pseudopotentials were quite satisfactory for our purposes.

IV. CONCLUSION

Our results explain the origin of the STEM observations on rare earth decoration of the prism planes of β-Si_3N_4 in terms of the stereochemical binding of rare earths to specific sites of the N-terminated grain surface. The presence and arrangement of undercoordinated N atoms on the terminal plane is the greatest factor in determining the observed adsorbate decoration. The anion-terminated prism planes with rows of single-bonded N atoms (alternating with rows of double-bonded N atoms) parallel to the *z* axis (i.e., [0001]) present surfaces of active sites for cation attachment. This strong relationship between surface structure and adsorption properties is probably quite general and indicates how adsorption-related properties can be connected with the structural characteristics of the reinforcing grain surfaces in ceramics. First-principles results predict rare earth coordination with particular surface anion groups that saturate valence bands of both adsorbate and N atoms in a threefold group. At present, the locations of these interfacial *anions* are not imaged even with aberration-corrected STEM, but only the underlying Si columns to which they are attached. For this reason, the first-principles predictions are especially important in interpreting experimental images.

While the theoretical models used in this work serve only as starting points for devising models that include additional atoms of the IGF, the results compare surprisingly well with experiment. Clearly, further investigations are needed that include the effects of interactions between the atoms at the interface and those within the intergranular film, and this work is in progress.

ACKNOWLEDGMENTS

Research was supported by the Division of Materials Sciences and Engineering, U.S. Department of Energy under Contract No. DE-AC05-00OR22725 with UT-Battelle, LLC, and the European Community "Growth" Program, NANOAM Contract No. GRD2-200-3030351. K.v.B. was also supported by the Division of Scientific User Facilities, by appointment to the ORNL Postdoctoral Research Program administered jointly by ORNL and ORISE, and a Feodor-Lynen scholarship of the Alexander von Humboldt Foundation. N.S. was partly supported by Grant-in-Aid for Young Scientists (A) (Grant No. 20686042) from the Ministry of Education, Culture, Sports, Science and Technology (MEXT, Japan). The authors thank C. L. Fu and J. R. Morris for helpful comments on this paper.

*Deceased.
†Present address: Department of Chemical Engineering and Materials Science, University of California at Davis, Davis, California 95616, USA.

[1] M. V. Swain (volume editor), *Structure and Properties of Ceramics*, Materials Science and Technology Vol. 11, edited by R. W. Cahn, P. Hassen, and E. J. Kramer (VHC, New York, 1994).
[2] G. Petzow and M. Herrmann, *Structure and Bonding* (Springer-Verlag, Berlin, 2002), Vol. 102, pp. 50–167.
[3] H. Gu, R. M. Cannon, H. J. Seifert, M. J. Hoffmann, and I. Tanaka, J. Am. Ceram. Soc. **85**, 25 (2002).
[4] H. Gu, R. M. Cannon, and M. Rühle, J. Mater. Res. **13**, 376 (1998).
[5] M. J. Hoffmann, H. Gu, and R. M. Cannon, in *Interfacial Engineering for Optimized Properties II*, MRS Symposia Proceedings No. 586, edited by C. B. Carter, E. L. Hall, C. L. Briant, and S. Nutt (Materials Research Society, Pittsburgh, 2000), pp. 65–74.
[6] M. Kitayama, K. M. Hirao, M. K. Toriyama, and S. J. Kanzaki, J. Ceram. Soc. Jpn. **107**, 995 (1999).
[7] P. F. Becher, G. S. Painter, E. Y. Sun, C. H. Hsueh, and M. J. Lance, Acta Mater. **48**, 4493 (2000).
[8] L. Wang, T.-Y. Tien, and I.-W. Chen, J. Am. Ceram. Soc. **86**, 1578 (2003).
[9] R. L. Satet and M. J. Hoffmann, Key Eng. Mater. **265-268**, 775 (2004).
[10] *Silicon Nitride Ceramics: Scientific and Technological Advances*, MRS Symposia Proceedings No. 287, edited by I.-W. Chen, P. F. Becher, M. Mitomo, G. Petzow, and T.-S. Yen (Materials Research Society, Pittsburgh, 1993).
[11] H.-J. Kleebe, J. Ceram. Soc. Jpn. **105**, 453 (1997).
[12] P. F. Becher, G. S. Painter, N. Shibata, H.-T. Lin, and M. K. Ferber, Key Eng. Mater. **287**, 233 (2005).
[13] H.-J. Kleebe, M. J. Hoffmann, and M. Ruehle, Z. Metallkd. **83**, 610 (1992).
[14] P. F. Becher, G. S. Painter, N. Shibata, S. B. Waters, and H.-T. Hua-Tay Lin, J. Am. Ceram. Soc. **91**, 2328 (2008).
[15] M. Kitayama, K. Hirao, and S. Kanzaki, J. Am. Ceram. Soc. **89**, 2612 (2006).
[16] E. Tani, K. Umebayashi, K. Kishi, and K. Kobayashi, Am. Ceram. Soc. Bull. **65**, 1311 (1986).
[17] P. F. Becher, E. Y. Sun, K. P. Plucknett, K. B. Alexander, C.-H. Hsueh, H.-T. Lin, S. B. Waters, C. G. Westmoreland, E.-S. Kang, K. Hirao, and M. Brito, J. Am. Ceram. Soc. **81**, 2821 (1998).
[18] K. Hirao, M. Ohashi, M. Brito, and S. Kansaki, J. Am. Ceram. Soc. **78**, 1687 (1995).
[19] R. L. Satet and M. J. Hoffmann, J. Eur. Ceram. Soc. **24**, 3437 (2004).
[20] A. Ziegler, C. Kisielowski, M. J. Hoffmann, and R. O. Ritchie, J. Am. Ceram. Soc. **86**, 1777 (2003).
[21] P. F. Becher, J. Am. Ceram. Soc. **74**, 255 (1991).
[22] M. Krämer, D. Wittmüss, H. Küppers, M. Hoffmann, and G. Petzow, J. Cryst. Growth **140**, 157 (1994).
[23] N. Shibata, S. J. Pennycook, T. R. Gosnell, G. S. Painter, W. A. Shelton, and P. F. Becher, Nature (London) **428**, 730 (2004).
[24] A. Ziegler, J. C. Idrobo, M. K. Cinibulk, C. Kisielowski, N. D. Browning, and R. O. Ritchie, Science **306**, 1768 (2004).
[25] G. B. Winkelman, C. Dwyer, T. S. Hudson, D. Nguyen-Manh, M. Döblinger, R. L. Satet, M. J. Hoffmann, and D. J. H. Cockayne, Philos. Mag. Lett. **84**, 755 (2004).
[26] G. B. Winkelman, C. Dwyer, T. S. Hudson, D. Nguyen-Manh, M. Döblinger, R. L. Satet, M. J. Hoffmann, and D. J. H. Cockayne, Appl. Phys. Lett. **87**, 061911 (2005).
[27] N. Shibata, G. S. Painter, R. L. Satet, M. J. Hoffmann, S. J. Pennycook, and P. F. Becher, Phys. Rev. B **72**, 140101(R) (2005).
[28] K. van Benthem, G. S. Painter, F. W. Averill, S. J. Pennycook, and P. F. Becher, Appl. Phys. Lett. **92**, 163110 (2008).
[29] R. Satet, Ph.D. dissertation, University of Karlsruhe, 2003.
[30] G. S. Painter, P. F. Becher, W. A. Shelton, R. L. Satet, and M. J. Hoffmann, Phys. Rev. B **70**, 144108 (2004).
[31] I. Tanaka, K. Niihara, S. Nasu, and H. Adachi, J. Am. Ceram. Soc. **76**, 2833 (1993).
[32] T. Nakayasu, T. Yamada, I. Tanaka, H. Adachi, and S. Goto, J. Am. Ceram. Soc. **81**, 565 (1998).
[33] G. S. Painter, P. F. Becher, H.-J. Kleebe, and G. Pezzotti, Phys. Rev. B **65**, 064113 (2002).
[34] X. Su and S. H. Garofalini, J. Mater. Res. **19**, 752 (2004).
[35] P. Rulis, J. Chen, L. Ouyang, W.-Y. Ching, X. Su, and S. H. Garofalini, Phys. Rev. B **71**, 235317 (2005).
[36] J. P. Perdew, K. Burke, and M. Ernzerhof, Phys. Rev. Lett. **77**, 3865 (1996).
[37] G. Kresse and J. Furthmüller, Comput. Mater. Sci. **6**, 15 (1996).
[38] G. Kresse and D. Joubert, Phys. Rev. B **59**, 1758 (1999).
[39] H. J. Monkhorst and J. D. Pack, Phys. Rev. B **13**, 5188 (1976).
[40] E. Voloshina and B. Paulus, J. Comput. Chem. **29**, 2107 (2008).
[41] S. Kalvoda, M. Dolg, H.-J. Flad, P. Fulde, and H. Stoll, Phys. Rev. B **57**, 2127 (1998).
[42] T. Suehiro, N. Hirosaki, Y. Yamamoto, T. Nishimura, M. Mitomo, J. Takahashi, and H. Yamane, J. Mater. Res. **19**, 959 (2004).
[43] F. W. Averill and G. S. Painter, Phys. Rev. B **50**, 7262 (1994).
[44] F. W. Averill and G. S. Painter, Phys. Rev. B **73**, 235125 (2006).
[45] P. Yang, H.-K. Fun, I. A. Rahman, and M. I. Saleh, Ceram. Int. **21**, 137 (1995).
[46] Calculations show that RE bond positions in the *x*-*y* plane of this unit cell are more stable than corresponding sites in a unit cell displaced by $z=u/2$, where u is the unit-cell width (symmetry translation displacement along the z axis in Fig. 1). Only one single-bonded nitrogen lies in the *x*-*y* plane of this latter cell, and binding of an adsorbate to it will be much weaker than for an adsorbate that bridges a pair of such atoms in the chosen cluster in Fig. 1.